Supplementary Information

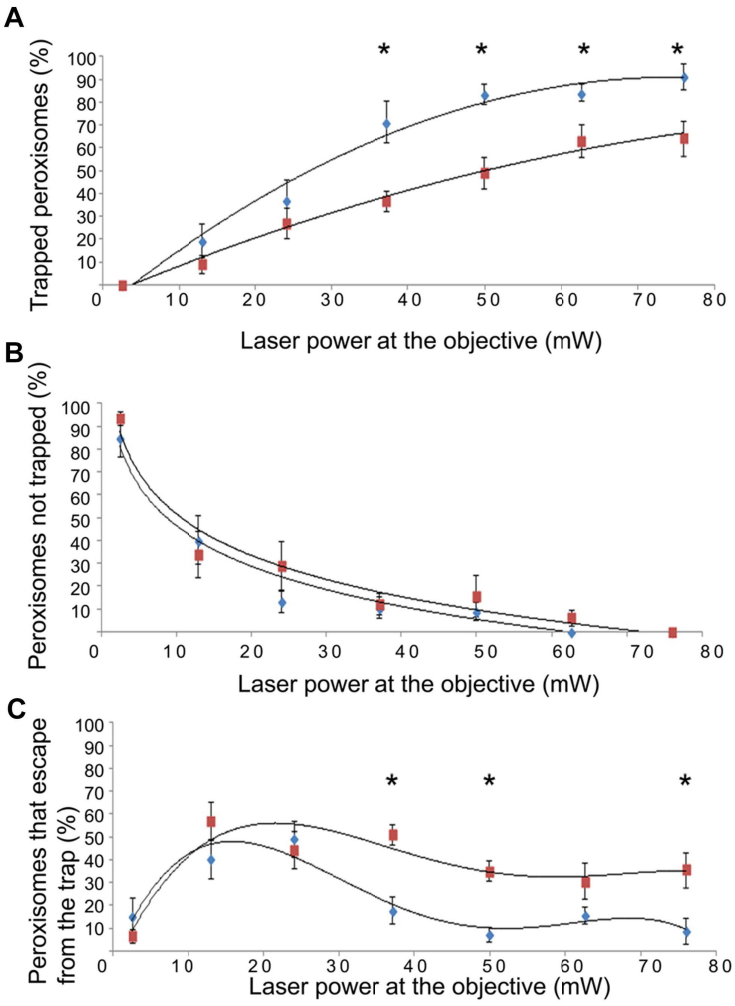

Figure S1: Relationship between cp and non-cp peroxisomal behaviour in the optical trap. Direct comparisons between cp (red) and non-cp (blue) peroxisome behaviour in the optical trap as a function of optical laser trap power; trapped (A), not trapped (B) and escaped the trap (C). Significant differences between chloroplast associated versus non associated at certain laser powers are denoted (Welchs T-test, $p < 0.05^{*}$). Weighted average S.E. are plotted; samples sizes are given in the materials and methods.

Supplementary Note. Spring Model of Peroxisome Motion

Model Overview: Our conceptual simplified model of peroxisome motion is based on the motion of a mass on a spring damped by viscous drag. First, we estimate the the Reynolds number of the flow and conclude that a laminar flow regime exists around the peroxisome. Second, we develop a model for the observed peroxisome motion using the force balance between inertial forces (Newton's second law), viscous drag forces (Stokes' law), and tether tension forces (Hooke's law). Finally, we fit the unknown model parameters: the viscosity-scaled spring constant k/μ and the recovery displacement b. These model parameters are well constrained by the experimental data. However, determination of the absolute sub-cellular forces and tether spring constants require the use of viscosity μ estimates from the literature, which contain considerable uncertainties when extrapolated to our experimental system. Details of the model and fitting technique are expanded upon below.

Model Setup: The model assumes that we can approximate the system using a spherical peroxisome moving in a Newtonian viscous fluid tethered to a base (anchor point) with a linear spring: the assumption of a Newtonian fluid is consistent with the linear trend observed in Figure S2 to within the experimental errors, allowing simple approximation of the viscous forces; and a spherical peroxisome shape is broadly consistent with our experimental observations (Figure 1). The base of the tether is assumed to be able to move during stage translation, but is then assumed to remain in a fixed position once stage translation has stopped. This is consistent with the limited amount of movement of the peroxule tip observed during recovery. When the trap is released, the peroxisome's recovery motion is driven by the net force due to the extended spring/tether and viscous drag. A schematic of the model is shown in Figure S3. This is the simplest possible model, with the fewest free parameters, that can be used to model the peroxisome recovery. A more advanced treatment incorporating non-linear tether properties or more complex cytoplasm properties (e.g. viscoelasticity or anisotropy) would require much more detailed constraints on cell properties than are currently available.

To determine the viscous drag force we must first determine if laminar or turbulent flow is occurring. Consider a spherical peroxisome of radius r moving in a viscous medium with dynamic

viscosity μ and density ρ_f at a representative velocity v. The flow regime can be estimated using the Reynolds number (Faber, 1995), which gives a measure of the ratio of inertial to viscous forces:

$$R_e = \frac{vL\rho_f}{\mu} \tag{1}$$

where L is a characteristic length scale of the flow, which can be approximated by the peroxisome diameter ($2r$). For our experiment: the cytoplasm density is $\approx$1000 Kg m^{-3}, the peroxisome radius was measured to be in the range 0.9–3.0 μm, and typical velocities were of order 1 μms^{-1}. Unfortunately, the cytoplasm viscosity in tobacco leaf epidermal cells has not been measured and is currently unknown. However, for our experimental scales (micron-sized spheres) a viscosity of 0.06 Pa s is reasonable based on measurements close to the nucleus and vacuole in chara (Scherp and Hasenstein, 2007), although extrapolation of this value to tobacco leaves is likely to introduce an order of magnitude uncertainty. Including the large uncertainty in viscosity and the full range of measured radii, our experimental regime has extremely small Reynolds numbers of $R_e = 10^{-9}$–10^{-6}.

This is well within the $R_e \ll 1$ criteria for a Stokes (or creeping) laminar flow. Therefore, the viscous drag on a peroxisome of radius r and velocity $\dot{x} = dx/dt$ can be estimated using Stokes' law:

$$F_{\text{drag}} = -6\pi\mu r\dot{x} \tag{2}$$

The negative sign is because the drag force is in the opposite direction to displacement x. The force due to the tether can be estimated using Hooke's law:

$$F_{\text{tether}} = +k(b-x) \tag{3}$$

where k is the spring constant (or stiffness) of the tether and $b-x$ is its extension (Figure S3).

Derivation of Peroxisome Equation of Motion: Assuming that the tether acts as a linear spring that obeys Hooke's law (tension force proportional to extension) and that the viscous drag is given by Stokes' law, Newton's second law (Force=mass$\times$acceleration) can be used to relate the accel-

eration of the peroxisome ($\ddot{x} = d^2x/dt$) to the net force ($F_{\text{tether}} + F_{\text{drag}}$):

$$m\ddot{x} = k(b-x) - 6\pi\mu r\dot{x} \tag{4}$$

Where m is the effective mass of the peroxisome, which is equal to the mass of the peroxisome plus half the mass of the displaced fluid. The additional mass is necessary to account for acceleration of the displaced fluid during recovery (Faber, 1995). However, for extremely low Reynolds numbers, as in our case, the inertial term ($m\ddot{x}$) is negligible compared to the viscous drag and tension forces. This simplifies the model considerably and gives a force balance of:

$$0 = k(b-x) - 6\pi\mu r\dot{x} \tag{5}$$

This first order differential equation can be solved by integration, using the boundary condition $x = 0$ at $t = 0$, to give the peroxisome equation of motion:

$$x(t) = b(1 - e^{-\frac{kt}{6\pi\mu r}}) \tag{6}$$

This model for the peroxisome motion has two free parameters: b the recovery displacement; and k/μ the ratio of the spring constant to the dynamic viscosity.

To find the best fitting parameters we perform a grid search over a wide range of b and k/μ in order to minimise the misfit χ^2 (Bevington and Robinson, 1992) between the model $x(t_i)$ and the data points $x_{\text{obs}}(t_i)$ defined at n time points t_i where $i = 1 \ldots n$:

$$\chi^2 = \sum_{i=1}^{n} (x(t_i) - x_{\text{obs}}(t_i))^2 \tag{7}$$

The optimal solution is given by the values of b and k/μ that minimise χ^2, where this minimum value is referred to as χ_0^2. To place estimated statistical limits on the solution, we derive effective uncertainties on the datapoints by requiring that $\chi_0^2/n = 1$ for the optimum solution (i.e. that the model is capable of fitting the data to within the errors). The inferred error-bars σ on the measured displacements are then given by $\sigma = \sqrt{\chi_0^2/n}$. For a two parameter (i.e. two degrees of freedom)

model the 3-σ (99.7% confidence) range of solutions is bounded by $\chi^2/\sigma^2 < \chi_0^2/\sigma^2 + 11.8$ (Press et al., 1992). This criteria can be used to ensure that the solutions are well constrained. Example fits of the model to the data are shown in Figure S4.

Note that while k/μ is well determined, the order of magnitude uncertainty in the viscosity μ means that absolute values for the spring constant and forces also contain an order of magnitude uncertainty.

Model Fitting Results: The motion of all 243 trapped peroxisomes (cp and non-cp combined) that could be tracked during the recovery period were fitted using the model. The model fits to each dataset were visually inspected to ensure that: (1) the simple motion predicted by the model adequately described the peroxisome motion; (2) the model fitted the measured data well; and (3) there were no discontinuities in the data caused by pixel-noise in the automated tracking process. Only those fits that passed this quality control process were considered suitable for further analysis.

We found that 32% of the data were fitted well by the model (n=25 chloroplast associated and n=52 non associated measurements). The remaining 68%, while having the gross recovery profile fitted by the model, had additional features that were not fitted by the model, such as intermittent changes in direction (eg Fig S4d) or an initial slow phase. This suggests that for these data peroxisome recovery was affected by unlabelled (i.e. non fluorescent) structures within the cell which physically impede motion or imaging problems (see above). In addition, several data were discarded due to peroxisomal signal saturation affecting the measurement of the radius (n=4 cp and n=9 non-cp). Even though the model grossly simplifies the system it can accurately reproduce the recovery motion in over 30% of cases. Figure 4 shows cumulative distribution functions of the model parameters for fits that passed the quality control criteria.

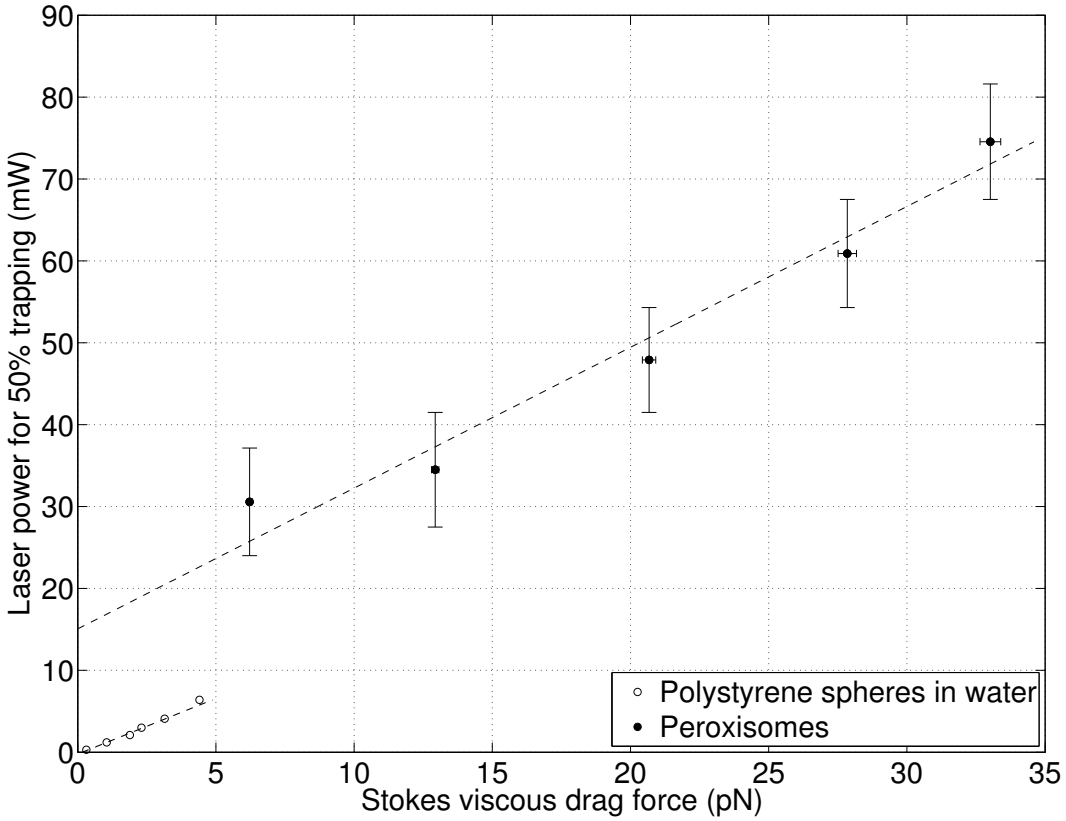

Figure S2: Laser power required for trapping peroxisomes and polystyrene beads at different stage velocities.

The drag force was determined from the stage velocity, particle radius, and viscosity using Stokes' law. For both 1 μm diameter polystyrene beads in water and $\approx$2 μm diameter peroxisomes in cytoplasm, there is a linear relation between viscous drag force and laser power, with a gradient of 1.36 mW/pN for beads and 1.72 mW/pN for peroxisomes. For peroxisomes, the error bars relate to the range of laser powers required to trap 30-80 separate peroxisomes of varying size. For polystyrene beads in water the intercept on the laser power axis is approximately zero as the beads were untethered. However, for peroxisomes a minimum laser power of $\approx$15 mW is required to overcome the tethering forces, resulting in a vertical offset of the datapoints. The linear force-power relation for peroxisomes implies that the viscous drag is linearly related to velocity and therefore that viscous forces can be adequately estimated assuming a Newtonian viscosity to within experimental errors.

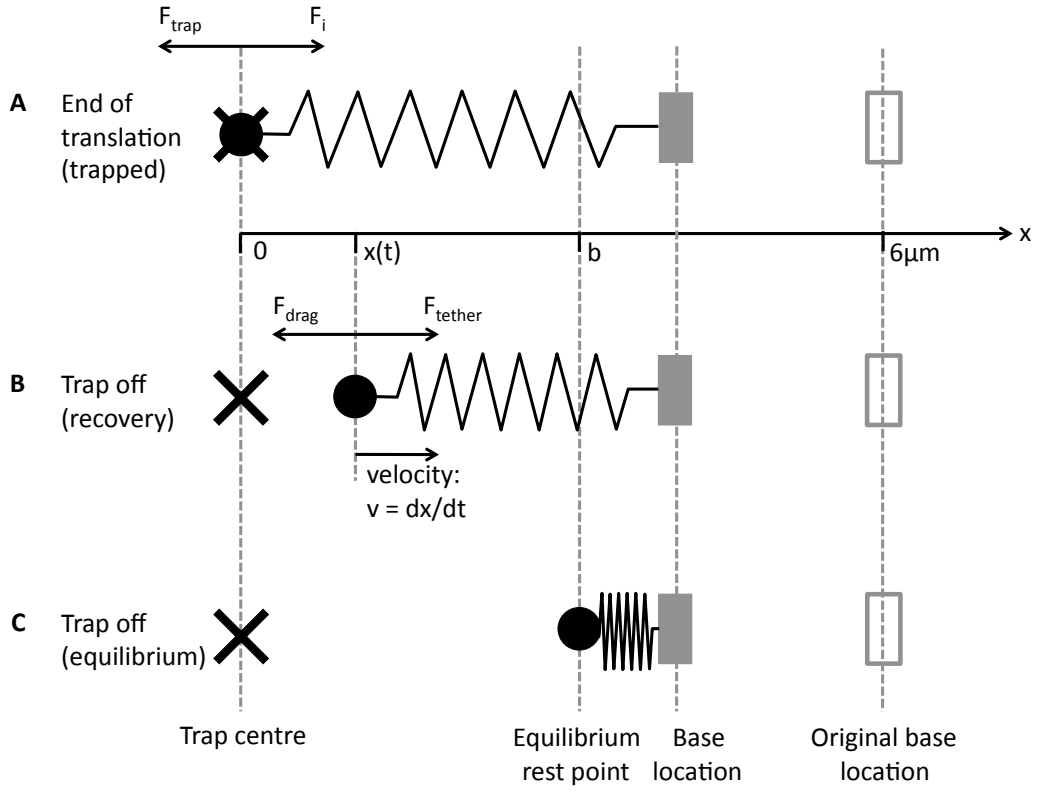

Figure S3: Spring model definition.

(A) At the end of translation, the peroxisome (black circle) is trapped such that the tether is extended relative to its unstressed length by an initial amount b. The tether is assumed to be attached to a base (grey rectangle) and is assumed to obey Hooke's law with a spring constant of k. The initial recovery force (F_i) exerted by the spring in this steady state from Hooke's law is F_i=kb and is counteracted by the laser trapping force F_{trap}. (B) When the trap is turned off, the recovery phase begins, where the peroxisome moves back toward its equilibrium/rest position. The position of the peroxisome $x(t)$ at time t is defined relative to the position of the trap centre (cross) for consistency with the experimental displacement measurements. During this motion the peroxisome experiences a tension force from the tether $F_{\text{tether}} = k(b-x)$ towards the base and a viscous drag force $F_{\text{drag}} = 6\pi\mu rv$ in the opposite direction, where v is peroxisome velocity (dx/dt). (C) Finally the tether has contracted to its unstressed length and the peroxisome has moved to its equilibrium position. The displacement at this equilibrium position is equal to b; the recovery displacement.

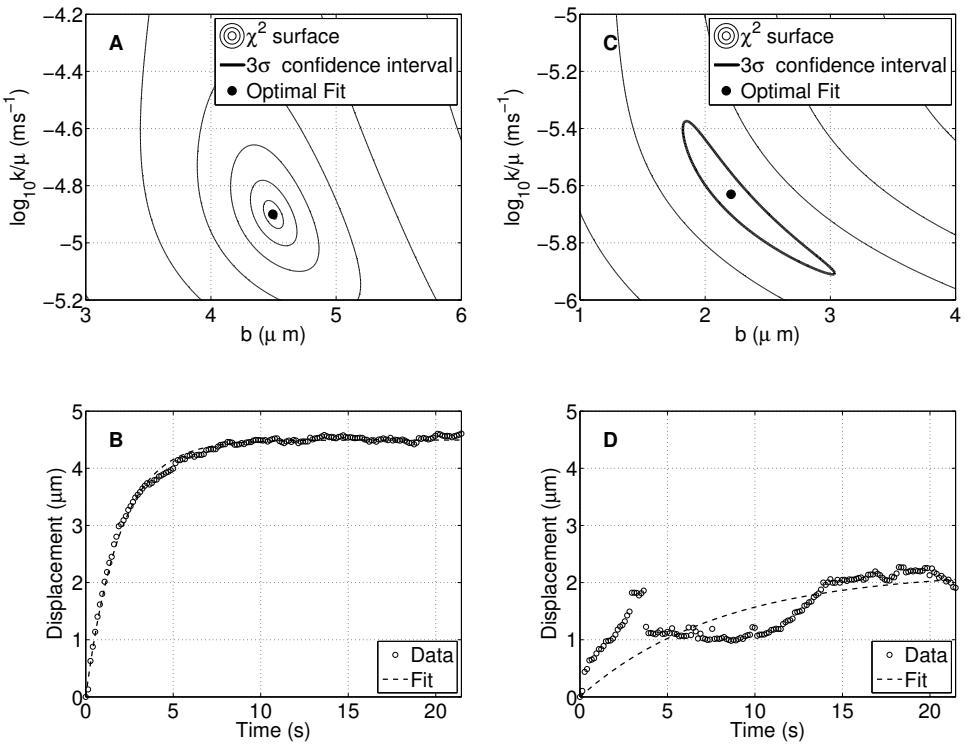

Figure S4: Example fits to the data using the simple spring model.

(A,B) Show a result where the simple spring model provides a good fit to the measured peroxisome recovery, whereas (C,D) show a result where the spring model does not adequately fit the peroxisome recovery. For each track a grid search over values of b from 0–10 μm and k/μ from 10^{-8}–10^{-2} ms^{-1} was performed to find the optimum fitting model parameters, which correspond to the minimum value of the χ^2 misfit. (A) and (C) show χ^2 contours around the region of best fit; the thick contour represents the 3-σ confidence interval on the model parameters, which is well defined and very compact in (A), indicating a good fit, and extended in (C), indicating a poor fit. The example in (A,B) has fit parameters of k/μ=1.25$\pm$0.04$\times 10^{-5}$ ms^{-1}, which assuming a viscosity of 0.06 Pa s implies k=0.8 pN/μm and F_i=3 pN (both with uncertainties of up to an order of magnitude). The example in (C,D) was rejected by the quality control procedure as the model does not fit the recovery curve well and the confidence interval on the optimum fit parameters is too large. These examples are for non-chloroplast associated peroxisomes.

Optical trapping power (mW)	76	63	50	37	24	13	Total *(%)*
CP							
Total number of trapped peroxisomes *(%)*	28 *(100)*	34 *(100)*	28 *(100)*	29 *(100)*	26 *(100)*	25 *(100)*	170 *(100)*
Total number of peroxisomes which produced peroxules *(%)*	8 *(28.6)*	11 *(32.4)*	14 *(50)*	13 *(44.8)*	12 *(46.2)*	6 *(24.0)*	64 *(37.6)*
Number of peroxisomes which produce peroxules;							
-before peroxisome translation *(%)*	0 *(0)*	0 *(0)*	2 *(7.1)*	3 *(10.3)*	0 *(0)*	0 *(0)*	5 *(2.9)*
-during peroxisome translation *(%)*	8 *(28.6)*	7 *(20.6)*	6 *(21.4)*	9 *(31.0)*	12 *(46.2)*	6 *(24.0)*	48 *(28.2)*
-ambiguous *(%)*	0 *(0)*	4 *(11.8)*	6 *(21.4)*	1 *(3.4)*	0 *(0)*	0 *(0)*	11 *(6.5)*
NON-CP							
Total number of trapped peroxisomes *(%)*	31 *(100)*	31 *(100)*	29 *(100)*	30 *(100)*	32 *(100)*	30 *(100)*	183 *(100)*
Total number of peroxisomes which produced peroxules *(%)*	9 *(29.0)*	11 *(35.5)*	13 *(44.8)*	18 *(60.0)*	11 *(34.4)*	6 *(20.0)*	68 *(37.2)*
Number of peroxisomes which produce peroxules;							
-before peroxisome translation *(%)*	0 *(0)*	1 *(3.2)*	8 *(27.6)*	7 *(23.3)*	5 *(15.6)*	1 *(3.3)*	22 *(12.0)*
-during peroxisome translation *(%)*	2 *(6.5)*	6 *(19.4)*	2 *(6.9)*	9 *(30)*	4 *(12.5)*	5 *(16.7)*	28 *(15.3)*
- ambiguous *(%)*	7 *(22.6)*	4 *(12.9)*	3 *(10.3)*	2 *(6.7)*	2 *(6.3)*	0 *(1.1)*	18 *(9.8)*

Table S1: Relationship between optical laser trap power and peroxule formation characteristics from cp and non-cp peroxisomes.

Peroxules were defined as a narrow tubular protrusion whose length was at least the same diameter as the trapped peroxisome. Potential problems with classifying peroxule formation were as follows; upon trapping and moving a peroxisome occasionally it appeared as though potentially two peroxisomes may have been closely associated resulting in a "beaded" appearance of the per-

oxule. Similar observations have been made from studies of peroxule formation from peroxisomes in *Arabidopsis* (Sinclair et al., 2009). In addition, peroxules also appeared to form sometime after the translation, which could have been a result of movement of the peroxule into the TIRF focal plane towards the end of the video, or diffusion, and subsequent detection, of the soluble luminal marker into the peroxule. Note, very occasionally, multiple peroxules emanated from the trapped organelle. Peroxisomes which were either trapped or escaped the trap were observed and those which displayed peroxules were categorised into either (1) formation upon trapping prior to the translation event (and therefore could be due to exposure to the trapping laser), (2) formation upon / during the 6 μm translation movement event, or (3) an ambiguous grouping. The latter includes peroxule formation sometime after the translation, or generation of beaded / two peroxisomes in the trap, and so could not be accurately used to determine whether peroxule formation was a direct result of exposure to the trapping laser or through subsequent micromanipulation and movement. Here, we used the fully automated dataset used to generate the data for Figure 2 where variable trapping laser strength was implemented. Numbers are absolute with percentages in brackets.

Movie S1. Peroxisome association with chloroplasts.

Time lapse images were taken of peroxisomes (green), Golgi (cyan) and chloroplasts (magenta) in tobacco leaf epidermal cells. Organelles were visualised through transient expression of fluorescent fusions (YFPSKL for peroxisomes and STCFP for Golgi bodies) or autofluorescence (chloroplasts). Compared to Golgi, peroxisomes spend longer periods of time associated with chloroplasts. The peroxisome appears tethered to a fixed zone on the surface of the chloroplast as the chloroplast moves (A), and in some cases the peroxisomes can also move laterally over the surface (B). Scale bar 5 μm.

Movie S2. Peroxisomes can be trapped and moved laterally within tobacco leaf epidermal cells.

Peroxisomes were trapped (arrowhead) and the stage moved 6 μm horizontally. During the translation peroxisomes either escaped the trap (A,C) or were moved 6 μm (B,D). Upon turning the trap off the peroxisomes moved back towards their original position (B,D). Peroxisomes juxtaposed to

chloroplasts (C,D) behaved similarly to peroxisomes which were not (A,B). In both cases, peroxules were observed (B,D) Scale bar 6 μm.

Movie S3. Peroxisome behaviour in the optical trap under actin depolymerisation.
A trapped non-cp (A) and cp (B) peroxisome undergoes the 6 μm translation resulting in peroxule formation. Upon turning the trap off the peroxisome moves back along the length of the peroxule. Movies highlighting examples of non-cp peroxisomes in tobacco leaf epidermal cells which are either (C) trapped, (D) not trapped (E) or escape the trap over the translation period. The samples were treated with latrunculin B and so any subsequent motion upon turning the trap off is independent of acto-myosin. Scale Bar 6 μm. Arrow head denotes peroxisome undergoing the trapping routine.

References

Bevington, P.R., Robinson, D.K., 1992. Data reduction and error analysis for the physical sciences. WBC/McGraw-Hill, New York. 2nd edition.

Faber, T.E., 1995. Fluid Dynamics for Physicists. Cambridge Univ. Press, Cambridge UK.

Press, W.H., Flannery, B.P., Teukolsky, S.A., Vetterling, W.T., 1992. Numerical Recipes. Cambridge Univ. Press, Cambridge UK. 2nd edition.

Scherp, P., Hasenstein, K.H., 2007. Anisotropic viscosity of the Chara (Characeae) rhizoid cytoplasm. Am. J. Bot. 94, 1930–1934.

Sinclair, A.M., Trobacher, C.P., Mathur, N., Greenwood, J.S., Mathur, J., 2009. Peroxule extension over ER-defined paths constitutes a rapid subcellular response to hydroxyl stress. Plant Journal 59, 231–242.